European Journal of Pain

ORIGINAL ARTICLE OPEN ACCESS

Astrocytic Inducible Nitric Oxide Synthase Upregulation Contributes to Chronic Below-Level Neuropathic Pain Following Spinal Cord Injury in Male Rats

Youngkyung Kim[1] | Hyunggoo Kang[2] | Young Wook Yoon[1]

[1]Department of Physiology, Korea University College of Medicine, Seoul, Republic of Korea | [2]Department of Emergency Medicine, College of Medicine, Hanyang University, Seoul, Republic of Korea

Correspondence: Young Wook Yoon (ywyoon@korea.ac.kr)

Received: 29 October 2024 | **Revised:** 24 April 2025 | **Accepted:** 16 May 2025

Funding: This work was supported by two separate grants from the Korea University (K2509181), and the Korea Science and Engineering Foundation (KOSEF), funded by the Ministry of Science and ICT (MSIT; Grant NRF-2022R1F1A1073548).

ABSTRACT

Background: Spinal cord injury (SCI) leads to persistent inflammation, contributing to chronic neuropathic pain. However, current treatments show limited efficacy. Three types of nitric oxide synthase (NOS) play different roles in inflammation and neuronal hyperexcitation. Therefore, this study aimed to determine the predominant NOS subtype involved in neuropathic pain after spinal contusion.

Methods: We investigated the effects of intrathecal NOS inhibitors on mechanical sensitivity following a moderate spinal contusion injury in male Sprague-Dawley rats. These NOS inhibitors were N(G)-nitro-L-arginine methyl ester hydrochloride (L-NAME; non-selective NOS inhibitor), 1400W (iNOS inhibitor), Nω-propyl-L-arginine hydrochloride (NPLA; nNOS inhibitor) and N5-(1-iminoethyl)-L-ornithine (L-NIO; eNOS inhibitor). Additionally, we analysed protein expression and cellular localisation of spinal NOS subtypes in rats that underwent SCI or sham procedures.

Results: Treatment with L-NAME significantly reduced paw withdrawal threshold in a dose-dependent manner, although motor deficits appeared at the highest dose (30 μM), while 1400W effectively alleviated mechanical hypersensitivity without motor side effects. NPLA showed limited efficacy, and L-NIO had no effect. Protein expression of iNOS increased two-fold in the L4-5 spinal segment of SCI rats compared with sham controls. After SCI, iNOS-immunoreactivity colocalized with GFAP in the superficial laminae of the L4-5 spinal segment. Treatment with 1400W reduced the hyper-reactivity of both iNOS and GFAP.

Conclusions: These findings indicate that iNOS plays a significant role in below-level neuropathic pain following thoracic spinal cord contusion in rats. Specific blockade of iNOS activity may have potential as a therapeutic intervention for spinal-contusion-induced neuropathic pain with reduced risk of side effects.

Significance Statement: iNOS inhibition effectively alleviated pain without motor side effects, unlike non-selective NOS, nNOS and eNOS inhibitors. The colocalization of iNOS with astrocytes in the spinal cord suggests a key mechanism in pain maintenance. These findings highlight the potential of targeting iNOS as a therapeutic strategy for SCI-induced neuropathic pain with reduced risks of side effects.

1 | Introduction

Traumatic spinal cord injuries (SCI) are more commonly observed in the working-age population, leading to extended periods of disability throughout the lifespan (Safdarian et al. 2023). The injury results in motor and sensory abnormalities below the injury site. Specifically, neuropathic pain occurring below the injury site is present in around 90% of patients in the chronic phase and significantly hinders progress in rehabilitation (Finnerup et al. 2014; Kim et al. 2020).

Propagated persistent inflammation throughout the majority of spinal segments contributes to neuropathic pain after SCI (Chambel et al. 2020; Li et al. 2022; Pfyffer et al. 2020; Varghese et al. 2024). However, corticosteroids, potent anti-inflammatory agents, show limited efficacy due to their indirect spinal cord action (Pertovaara and Breivik 2016), and the efficacy of minocycline was insufficient in a Phase II clinical trial (Casha et al. 2012). Thus, it is necessary to elucidate targets that can modulate neuropathic pain through the reduction of chronic inflammation in SCI.

L-Arginine is a crucial amino acid for immune cell activation during wound healing. It is converted to L-citrulline by nitric oxide synthase (NOS), resulting in the synthesis of nitric oxide (NO) (Arribas-López et al. 2021). NO is a vasodilator released from injured tissue and plays a role in recruiting inflammatory cells to the injured region (Andrabi et al. 2023). However, elevated levels of NO may readily combine with superoxide to generate peroxynitrites, leading to chronic inflammation and neuronal hypersensitivity (Doyle et al. 2012; Komirishetty et al. 2021; Lackovic et al. 2023). Therefore, the regulation of NO production via NOS is essential for developing potential therapeutic strategies for managing neuropathic pain (De Alba et al. 2006; Staunton et al. 2018; Thomas et al. 2001; Yoon et al. 1998).

There are three subtypes of NOS that differ in their cellular localization: neuronal NOS (nNOS), endothelial NOS (eNOS) and inducible NOS (iNOS) (Förstermann and Sessa 2012; Zhou and Zhu 2009). These subtypes play distinct roles depending on the stage of the inflammatory process and have been found to have different effects in injury models (Beck et al. 2004; Boettger et al. 2007; Freire et al. 2009; Yang et al. 2007). iNOS is upregulated by pro-inflammatory mediators and drastically increases NO production to more than 10 times the physiological level (Murphy et al. 1993; Zhao et al. 1998). Selective iNOS inhibition could reduce excessive NO concentrations while maintaining the basal NO levels through the constitutive nNOS and eNOS. In contrast, eNOS plays a protective role after SCI by enhancing intraspinal blood circulation and inhibiting pro-inflammatory reactions (Osuka et al. 2008; Paterniti et al. 2011), while nNOS is involved in the downstream signalling of NMDA receptors, which are crucial in central sensitization, a mechanism that induces neuropathic pain (Lee et al. 2018; Liang et al. 2021).

These differences in mechanisms lead to uncertainty regarding the predominant contributing NOS subtype to neuropathic pain following spinal contusion. To address this question, we compared the effects of three subtypes of NOS inhibitors on persistent below-level neuropathic pain after SCI.

2 | Materials and Methods

2.1 | Experimental Animals

All animal experimental procedures were conducted in accordance with the guidelines approved by the Institutional Animal Care and Use Committee of Korea University. We performed all experiments according to the relevant guidelines. In this study, we used 172 male Sprague–Dawley rats weighing 220–250 g. We purchased the rats from Charles River Laboratories (Orient Bio, Sungnam, Republic of Korea) and provided free access to water and food (5L79, Orient Bio, Republic of Korea) with a 12:12 h light cycle (day 8:00–20:00). All animals underwent an adaptation period for 1 week before experiments. The rats were randomly assigned to groups.

2.2 | Contusive Spinal Cord Injury

Contusive spinal cord injury was induced as described in our previous studies (Kim et al. 2012, 2023, 2019). In brief, the rats were anaesthetised under isoflurane inhalation (Hana Pharm, Hwaseong, Republic of Korea), and spinal contusion was induced by dropping a 10-g weight onto the spinal cord at the previously exposed T10 vertebra from a height of 12.5 mm using a New York University (NYU) impactor. The animals subcutaneously received normal saline for rehydration and 100 mg/kg of ampicillin/sulbactam (UNASYN, Pfizer, New York, NY, USA) to prevent urinary infections after the operation. Any rats able to perform hind limb joint motion or weight-supported locomotion immediately after the operation were excluded from this study.

2.3 | Insertion of the Intrathecal Cannula

The intrathecal cannulation procedure has been described in our previous studies (Kim et al. 2012, 2023). In brief, 3 weeks after undergoing the SCI operation, the rats were again anaesthetised with isoflurane and an 11 cm PE-10 polyethylene tube was advanced 5.5 cm into the subarachnoid space via the atlanto-occipital membrane. The external portion of the tube was used to administer the test drugs. Lidocaine was administered to confirm accurate placement of the tube, and hind limb paralysis was assessed as an indicator of proper insertion. Any rats showing neurological deficits during the 1-week recovery period after the operation were excluded from this study.

2.4 | Drug Administration

One week after placement of the cannular, vehicle or drug was administered through the intrathecal cannular using a Hamilton syringe. All drugs were dissolved in 0.9% saline (Vehicle, Daihan Pharmaceutical Co. Ltd., Ansan, Republic of Korea). The concentrations of the drugs applied intrathecally were as follows: Nω-Nitro-L-arginine methyl ester hydrochloride (L-NAME) at 5, 15 and 30 μM/5 μL (#N5751, Merk, Darmstadt, Germany); Nω-Nitro-D-arginine methyl ester hydrochloride (D-NAME) at 30 μM/5 μL (#21687, Cayman, Ann Arbor, USA); 1400W dihydrochloride at 10, 50 and 100 nM/5 μL (#1415, Tocris Bioscience, Bristol, UK); Nω-Propyl-L-arginine

hydrochloride (NPLA) at 50, 100, 200 nM/5 μL (#SML2341, Merk, Darmstadt, Germany); L-NIO dihydrochloride at 50, 100, 200 nM/5 μL (#0546, Tocris Bioscience, Bristol, UK); and L-. The cannula was flushed and filled with 10 μL of 0.9% normal saline after drug administration.

2.5 | Behaviour Tests

We measured paw withdrawal thresholds against mechanical stimuli and motor-related side effects before and 15, 30, 45, 60, 90, 120, 150 and 180 min after intrathecal drug administration at 4 weeks after SCI. Evaluation of the drug treatment results was conducted in a double-blind manner.

2.5.1 | Paw Withdrawal Threshold in Response to Mechanical Stimuli

The rats were placed on a wired mesh grid and hind paw withdrawal thresholds in response to mechanical stimuli were measured. The stimuli consisted of a series of 8 von Frey filaments with 3.61, 3.84, 4.08, 4.31, 4.56, 4.74, 4.93 or 5.18 mN target force ratings (Stoelting, Woodale, IL, USA) (Chaplan et al. 1994). The 4.31 mN filament was the starting force. If the rat shows a withdrawal response to the filament, the next stimulation will be applied with a force below this value. If the rat does not show a withdrawal response to the filament, the next stimulation will be applied with a force above this value. The stimulation was applied five times starting from the initial withdrawal response. The cut-off force was 5.18 mN.

2.5.2 | Combined Behavioural Score (CBS)

CBS includes a series of behavioural assessments related to motor function. Modified CBS was used to analyse motor function and reflexes of the hind limb (Gale et al. 1985). Normal rats were assigned a total score of 90, while rats showing complete paralysis were assigned a score of 0. A detailed description of how we calculated the CBS score is presented in Table 1.

TABLE 1 | CBS calculation.

	Point	Description
Motor Score		
0	0	Normal walking
1	5	Walks with only mild deficit
2	15	Hind limb can support weight
3	25	Frequent movement of hindlimb, no weight support
4	40	Minor movement in hind limb, no weight bearing
5	45	No movement in hindlimb, no weight bearing
Toe spread		
0	0	Normal full toe spread
1	2.5	Partial spreading of toe
2	5	No spreading of toe
Righting reflex		
0	0	Normal righting counter to direction of roll
1	5	Weakend attempt to right
2	10	Delayed attempt to right
3	15	Delayed attempt to right itself
Extension withdrawal		
0	0	Normal
1	2.5	Weak and slow reflex to withdraw the hindlimb
2	5	No withdrawal reflex
Placing		
0	0	Normal placing
1	2.5	Weak attempt to place foot
2	5	No attempt to place foot
Incline plate		
0	0	65-70/deg
1	5	55–60
2	10	40–50
3	15	< 40

2.6 | Tissue Collection

Tissue collection was performed as described in our previous report (Kim et al. 2023).

For western blotting, tissues from the T9-T10 (rostral region), T11-T12 (injured epicentre), L1-L2 (caudal region) and L4-L5 (remote site) in the spinal cord were collected after cardiac perfusion with 0.9% saline under general anaesthesia (alfaxalone-xylazine mixture) at 4 weeks after the sham and SCI operation. Samples were kept at −70°C until protein extraction for western blotting.

For histological experiments, perfusion with 4% paraformaldehyde was performed after blood removal. We collected the L4-L5 spinal segment at 1 h after the administration of iNOS inhibitor 1400W 100 nM/5 μL. After soaking with 30% sucrose, the tissues were embedded into an optimal cutting temperature compound (OCT, Tissue-Tek, Sakura Finetek, Torrance, CA, USA) and sectioned transversely at 14 μm thickness using a cryostat microtome (Leica CM3050S). The sections were attached to a coated slide glass (Platinum, Matsunami, Osaka, Japan).

2.7 | Western Blotting

We performed western blot as described in our previous report (Kim et al. 2023). In brief, proteins were extracted in lysis buffer with a 1×protease inhibitor cocktail (Halt Protease Inhibitor Cocktail, EDTA-free, Thermo Fisher Scientific, Waltham, MA, USA) using a homogeniser (PT1200E, Polytron, Switzerland). Denatured protein (50 μg) was separated by sodium dodecyl sulfate-polyacrylamide gel electrophoresis and electrophoretically transferred to a polyvinylidene fluoride membrane (IMMOBILION-P, Millipore, Burlington, MA, USA).

After blocking, the membrane was incubated with primary and secondary antibodies diluted in a 5% blocking buffer (232100, BD Difco, San Jose, CA, USA). The antibodies used are listed in Table 2. The membrane was washed with tris-buffered saline containing 0.75% Tween 20 after antibody incubation. The membrane was exposed to an X-ray film (CP-BU, Agfa, Mortsel, Belgium) after reaction with an enhanced chemiluminescence reagent kit (EZ-Western Lumi Pico, DG-WP100, Dogen, Seoul, Republic of Korea). The intensity of the immunoreactive band in the images obtained was assessed using ImageJ software (NIH, Bethesda, MD, USA). The band intensities were normalised to the corresponding intensity of the Ponceau S staining.

2.8 | Fluorescent Immunohistochemistry (IHC)

We performed IHC as described in our previous report (Kim et al. 2023). Rehydrated tissue slides were incubated with primary and secondary antibodies after blocking endogenous Fc binding activity with 10% normal goat serum (S1000, Vector Laboratories, USA). The antibodies used are listed in Table 2. A coverslip was mounted on each slide using Vectashield mounting medium with DAPI (H-1500, Vector Laboratories, USA).

Fluorescent images of the dorsal horn were obtained using a confocal microscope (LSM700, Carl Zeiss, Switzerland). A total of 30 sections were selected from three groups: sham-operated, 4-week SCI and 4-week SCI treated with 1400W (100 nmol/5 μL) groups (10 sections per group, 2 sections from each of 5 rats). Images were captured at 200× magnification. These sections were analysed using ImageJ software (NIH, Bethesda, MD, USA). To analyse astrocyte branch length, we utilised the method described by Marques et al. (2023). The GFAP staining of captured images was converted to skeletonized 8-bit format, and maximum branch length was calculated using the AnalyzeSkeleton plugin in ImageJ.

2.9 | Statistical Analysis

All statistical analyses were performed using SPSS Statistics 29.0 (IBM, USA). All data were analysed according to the results of the Shapiro–Wilks normality test. A two-way repeated measures analysis of variance (ANOVA) was used to compare drug-administered groups and the vehicle group depending on the time point, followed by Bonferroni's post hoc test (Greenhouse–Geisser corrected). The anti-nociceptive effects of the drugs at different doses were compared using the area under the curve (AUC) calculated by the trapezoidal rule based on %MPE (percent maximum possible effect). The %MPE was calculated as %MPE = (post-drug PWT− pre-drug PWT)/(15 g − pre-drug PWT)×100. A one-way ANOVA was used to analyse differences among drug doses in drug-administered groups. IHC data was analysed using one-way ANOVA and Western blot was analysed using the Mann–Whitney *U* test as described in our previous report (Kim et al. 2012). All data are presented as mean ± standard error of the mean (SEM). Statistical significance was considered at $p < 0.05$. Detailed statistical results for significant findings are presented in Table 3.

3 | Results

3.1 | Intrathecal Administration of the Non-Selective NOS Inhibitor L-NAME Reduces Mechanical Paw Hypersensitivity in a Dose-Dependent Manner in Rats With Spinal Contusion

We intrathecally administered vehicle (0.9% saline), D-NAME at 30 μM/5 μL or L-NAME at concentrations of 5, 15 and 30 μM/5 μL at 4 weeks after moderate spinal contusive injury. Mechanical withdrawal thresholds in response to stimuli were measured at 15-min intervals for up to 180 min following intrathecal administration. The main effect of time ($F(2.07, 8.3) = 4.68$, $p = 0.043$) was statistically significant by statistical analysis using two-way RM ANOVA.

TABLE 2 | Antibodies information used in this study.

Primary antibodies	First titre	Secondary antibodies	Second titre	
Rabbit polyclonal anti-iNOS (ab3523, Abcam, UK)	1:2000	Goat anti-Rabbit, HRP (WB-1000, Vector Lab, USA)	1:3000	WB
Rabbit monoclonal anti-nNOS (ab76067, Abcam, UK)	1:1000		1:2000	WB
Rabbit polyclonal anti-eNOS (ab5589, Abcam, UK)	1:1000		1:2000	WB
Rabbit polyclonal anti-iNOS (ab3523, Abcam, UK)	1:100	Goat anti-rabbit IgG, Alexa 594 (A32740, Thermo Fisher Scientific, USA)	1:100	IHC
Mouse monoclonal anti-NeuN (ab104224, Abcam, UK)	1:1500	Goat anti-mouse IgG, Alexa 488 (A32723, Thermo Fisher Scientific, USA)	1:3000	IHC
Mouse monoclonal anti-GFAP (ab4648, Abcam, UK)	1:2500		1:3000	IHC
Mouse monoclonal anti-OX-42 (ab1211, Abcam, UK)	1:100		1:1000	IHC

TABLE 3 | Detailed statistical results for significant findings in figures.

Figure	Analysis	Factor	Statics
Figure 1A	Two-way RM ANOVA	Time	$F(2.07, 8.3) = 4.68$, $p = 0.043$
		Time*Dose	$F = 3.27$, $p < 0.001$
	Post hoc: Bonferroni's	15 min: vehicle vs. 30 μM	$p = 0.010$
		30 min: vehicle vs. 15 μM	$p = 0.025$
		30 min: vehicle vs. 30 μM	$p < 0.001$
		45 min: vehicle vs. 30 μM	$p = 0.019$
		60 min: vehicle vs. 30 μM	$p = 0.003$
		90 min: vehicle vs. 30 μM	$p = 0.007$
		120 min: vehicle vs. 30 μM	$p = 0.019$
		150 min: vehicle vs. 30 μM	$p = 0.005$
		180 min: vehicle vs. 30 μM	$p < 0.001$
Figure 1B	One-way ANOVA		$F = 6.86$, $p < 0.001$
	Post hoc: Bonferroni's	Vehicle vs. 15 μM	$p = 0.016$
		Vehicle vs. 30 μM	$p = 0.002$
Figure 1C	Two-way RM ANOVA	Time	$F(1.95, 75.91) = 6.60$, $p = 0.002$
		Time*Dose	$F = 3.55$, $p = 0.002$
	Post hoc: Bonferroni's	150 min: vehicle vs. 30 μM	$p < 0.001$
Figure 2A	Two-way RM ANOVA	Time	$F(4.51, 148.65) = 29.05$, $p < 0.001$
		Time*Dose	$F = 7.64$, $p < 0.001$
	Post hoc: Bonferroni's	15 min: vehicle vs. 50 nM	$p = 0.016$
		15 min: vehicle vs. 100 nM	$p < 0.001$
		30 min: vehicle vs. 10 nM	$p = 0.048$
		30 min: vehicle vs. 50 nM	$p = 0.017$
		30 min: vehicle vs. 100 nM	$p < 0.001$
		45 min: vehicle vs. 50 nM	$p < 0.001$
		45 min: vehicle vs. 100 nM	$p < 0.001$
		60 min: vehicle vs. 50 nM	$p = 0.001$
		60 min: vehicle vs. 100 nM	$p < 0.001$
		90 min: vehicle vs. 50 nM	$p = 0.048$
		90 min: vehicle vs. 100 nM	$p < 0.001$
		120 min: vehicle vs. 50 nM	$p = 0.024$
		120 min: vehicle vs. 100 nM	$p < 0.001$
		150 min: vehicle vs. 100 nM	$p < 0.001$
Figure 2B	One-way ANOVA		$F = 25.024$, $p < 0.001$
	Post hoc: Bonferroni's	Vehicle vs. 50 nM	$p = 0.004$
		Vehicle vs. 100 nM	$p < 0.001$
		10 nM vs. 50 nM	$p = 0.013$
		10 nM vs. 100 nM	$p < 0.001$
		50 nM vs. 100 nM	$p < 0.001$

(Continues)

TABLE 3 | (Continued)

Figure	Analysis	Factor	Statics
Figure 3A	Two-way RM ANOVA	Time	$F(4.19, 113.09) = 27.33$, $p < 0.001$
		Time*Dose	$F = 3.58$, $p < 0.001$
	Post hoc: Bonferroni's	45 min: vehicle vs. 100 nM	$p = 0.018$
		45 min: vehicle vs. 200 nM	$p = 0.003$
Figure 5	Mann–Whitney	Sham vs. SCI	$p = 0.004$
Figure 6D	One-way ANOVA		$F = 10.223$, $p < 0.001$
	Post hoc: Bonferroni's	Sham vs. SCI	$p < 0.001$
		Sham vs. SCI+1400W	$p = 0.006$
Figure 6H	One-way ANOVA		$F = 21.456$, $p < 0.001$
	Post hoc: Bonferroni's	Sham vs. SCI	$p < 0.001$
		SCI vs. SCI+1400W	$p < 0.001$
	One-way ANOVA		$F = 56.402$, $p < 0.001$
	Post hoc: Bonferroni's	Sham vs. SCI	$p < 0.001$
		Sham vs. SCI+1400W	$p < 0.001$
		SCI vs. SCI+1400W	$p < 0.001$

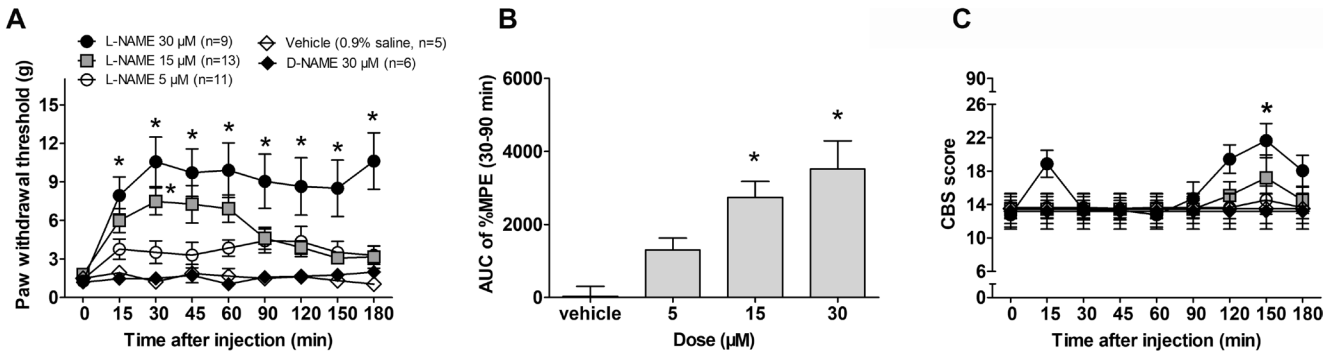

FIGURE 1 | Effect of intrathecal administration of the non-selective NOS inhibitor, L-NAME, on mechanical paw hypersensitivity in SCI rats. (A) Paw withdrawal thresholds in response to mechanical stimuli following intrathecal administration of vehicle (0.9% saline, open diamonds, $n = 5$), D-NAME at 30 µM/5 µL (closed diamonds, $n = 6$), L-NAME at 5 µM/5 µL (open circles, $n = 11$), 15 µM/5 µL (grey squares, $n = 13$) or 30 µM/5 µL (closed circles, $n = 9$) at 4 weeks post-SCI. (B) Area under the curve (AUC) calculated from the percentage of maximal possible effect (%MPE) for L-NAME treatment. (C) Motor-related side effects assessed by combined behavioural score (CBS) for L-NAME treatment. All data are presented as mean ± standard error of the mean (SEM). *$p < 0.05$: vehicle versus L-NAME treatment.

Prior to drug administration, the average withdrawal thresholds of both hind paws in 44 rats were 1.48 ± 0.09 g. The rats were randomly divided into treatment groups. Administration of 30 µM L-NAME significantly reduced paw hypersensitivity at all time points from 15 to 180 min after injection compared to the vehicle (0.9% saline), while 15 µM L-NAME significantly reduced the mechanical withdrawal threshold to 7.48 ± 1.05 g only at 30 min post-administration (Figure 1A). The effects of 5 µM L-NAME were not significantly different from the vehicle control (Figure 1A), nor was that of D-NAME at 30 µM, a stereoisomeric control for L-NAME.

The area under curve (AUC) for the %MPE increased in a dose-dependent manner, and significant differences were observed at 15 and 30 µM compared to the vehicle (Figure 1B $F = 6.86$, $p = 0.016$, $p = 0.002$, respectively). We analysed the AUC, specifically examining the time period between 30 and 90 min after the administration of L-NAME, during which no motor deficits were observed (Figure 1B). The data excluded at 15 min and after 120 min, because L-NAME at 30 µM resulted in partial motor impairment at 15 min post-injection, as well as from 120 min post-injection onwards (Figure 1C $F = (1.95, 75.91) = 6.60$, $p < 0.001$). This motor impairment may have contributed to the observed elevation in paw withdrawal thresholds at that time point.

The key finding of this result suggests that inhibiting NOS may decrease paw hypersensitivity, implying a potential role of NOS in the maintenance of neuropathic pain following spinal cord injury. As a result, our follow-up experiments concentrated on selectively blocking specific NOS subtypes.

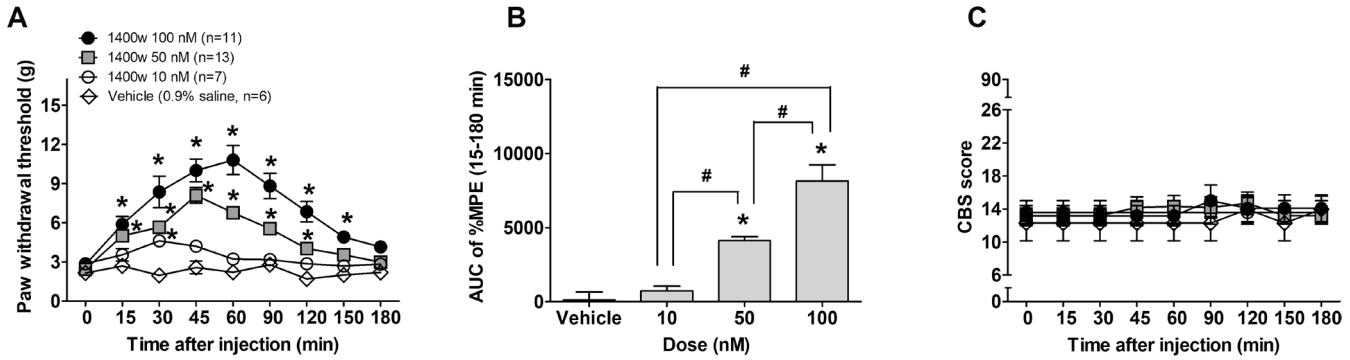

FIGURE 2 | Effect of intrathecal administration of the selective iNOS inhibitor 1400W on mechanical paw hypersensitivity in SCI rats. (A) Paw withdrawal thresholds in response to mechanical stimuli following intrathecal administration of vehicle (0.9% saline, open diamonds, $n=6$) or 1400W at 10 (open circles, $n=7$), 50 (grey squares, $n=13$) or 100 nM/5 μL (closed circles, $n=11$) at 4 weeks post-SCI. (B) AUC calculated from %MPE values. (C) Motor-related side effects assessed by CBS score. All data are presented as mean ± standard error of the mean (SEM). $^{*}p<0.05$: vehicle versus 1400W treatment, $^{\#}p<0.05$: pairwise comparison among the treated groups.

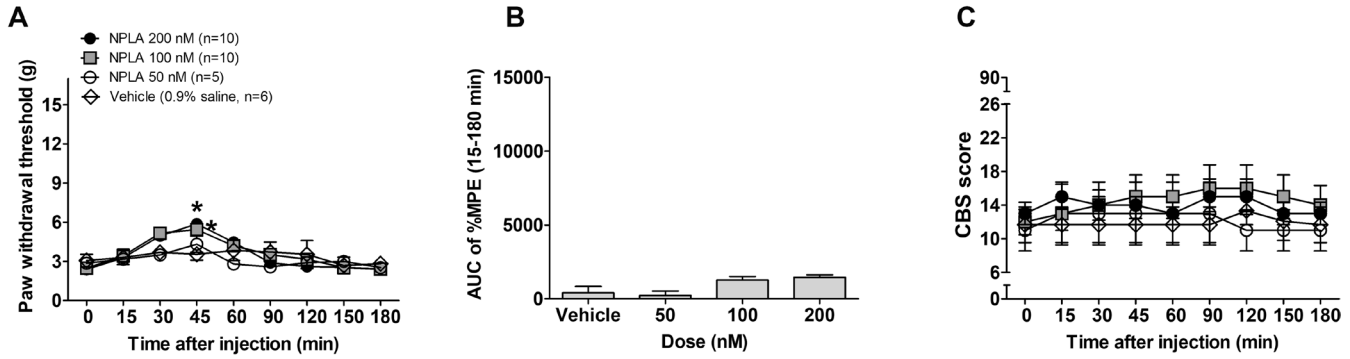

FIGURE 3 | Effect of intrathecal administration of the selective nNOS inhibitor NPLA on mechanical paw hypersensitivity in SCI rats. (A) Paw withdrawal thresholds in response to mechanical stimuli following intrathecal administration of vehicle (0.9% saline, open diamonds, $n=6$) or NPLA at 50 (open circles, $n=5$), 100 (grey squares, $n=10$) or 200 nM/5 μL (closed circles, $n=10$) at 4 weeks post-SCI. (B) AUC calculated from %MPE values. (C) Motor-related side effects assessed by CBS score. All data are presented as mean ± standard error of the mean (SEM). $^{*}p<0.05$: vehicle versus NPLA treatment.

3.2 | Intrathecal Administration of Selective iNOS Inhibitor 1400W Reduces Mechanical Paw Hypersensitivity Without Motor Deficits in Rats With Spinal Contusion

We measured the mechanical paw withdrawal thresholds in response to mechanical stimuli at 15-min intervals for up to 180 min after intrathecal administration of vehicle (0.9% saline) or 1400W at concentrations of 10, 50 and 100 nM/5 μL. The main effect of time (F (4.51, 148.65) = 29.05, $p<0.001$) was statistically significant by statistical analysis using two-way RM ANOVA. The baseline withdrawal thresholds of both hind paws in 37 rats averaged 2.59 ± 0.10 g. Paw hypersensitivity was significantly reduced at all time points from 15 to 120 min after administration of 50 nM 1400W and from 15 to 150 min after administration of 100 nM 1400W compared to the vehicle (0.9% saline) as shown in Figure 2A. At 10 nM, 1400W reduced paw hypersensitivity at the 30-min time point (Figure 2A $p=0.048$).

We calculated the AUC of the %MPE between 15 and 180 min after 1400W administration. The AUC values were significantly different from those for the vehicle at 50 and 100 nM (Figure 2B $F=25.024$, $p=0.004$, $p<0.001$, respectively). There were also significant differences between the drug treatment groups, indicating a dose-dependent effect (Figure 2B). Furthermore, intrathecally administered 1400W did not cause any motor deficits at any of the doses tested (Figure 2C).

3.3 | Intrathecal Administration of the Selective nNOS Inhibitor NPLA Exhibits Limited Efficacy in Reducing Mechanical Hypersensitivity Without Motor Deficits in Rats With Spinal Contusion

The mechanical withdrawal thresholds were measured at 15-min intervals for up to 180 min after intrathecal administration of NPLA at concentrations of 50, 100 and 200 nM/5 μL. The NPLA compound, known to have a Ki value of 50 nM, was initially administered at the same concentration. The main effect of time (F (4.19, 113.09) = 27.33, $p<0.001$) was statistically significant by statistical analysis using two-way RM ANOVA.

The baseline withdrawal thresholds of both hind paws in 31 rats averaged 2.62 ± 0.17 g. Administration of 100 or 200 nM NPLA significantly increased paw withdrawal thresholds to 5.44 ± 0.38 ($p=0.018$) and 5.87 ± 0.28 g ($p=0.003$), respectively, but only at 45 min after administration (Figure 3A). Importantly, there was no observable dose-dependent relationship between concentrations of 100 and 200 nM, suggesting that higher doses were unnecessary due to a slight motor impairment, albeit not statistically significant.

The AUC of the %MPE as calculated for time points between 15 and 180 min after NPLA administration was not significantly different from that for the vehicle control (Figure 3B). Intrathecally administered NPLA did not produce any significant motor deficits at any of the doses tested (Figure 3C).

3.4 | Intrathecal Administration of the eNOS Inhibitor L-NIO Produced No Effect on Mechanical Hypersensitivity or Motor Function in Rats With Spinal Contusion

The mechanical withdrawal thresholds were measured at 15-min intervals for up to 180 min after intrathecal administration of L-NIO at concentrations of 50, 100 and 200 nM/5 μL. In the context of L-NIO, with a Ki value of 3.9 μM, doses up to 200 nM were administered, representing a concentration almost 20 times lower. This decision was made in light of prior research indicating that L-NIO at a concentration of 2 μM results in focal cerebral ischemia in rats (Van Slooten et al. 2015).

The results indicated that L-NIO did not affect paw hypersensitivity at any time point compared with the vehicle control (Figure 4A). Additionally, there were no significant changes in the AUC of %MPE or motor-function-related side effects at any of the doses tested (Figure 4B,C). Since there was no observed elevation in eNOS protein expression in the spinal cord, we hypothesised that higher concentrations would elevate the likelihood of adverse side effects without imparting extra therapeutic advantages.

3.5 | Persistent iNOS Upregulation in Remote Spinal Segments Contributes to Chronic Mechanical Hypersensitivity After SCI

We analysed protein expression of the three types of NOS in the rostral (T9-T10), epicentre (T11-T12), caudal (L1-L2) and remote site (L4-L5) of the spinal cord 4 weeks after spinal contusion in rats. Protein expression of iNOS increased 2-fold in the L4-L5 spinal segment of rats with experimental spinal contusion compared with sham-operated rats ($p = 0.004$), while nNOS and eNOS showed no significant differences (Figure 5A,B). These results suggest that spinal contusion-induced iNOS activity may persist in regions distant from the injury site, such as the L4-L5, even as much as 4 weeks after the initial injury, potentially contributing to the observed mechanical hypersensitivity in areas innervating the hind paws.

3.6 | Spinal-Contusion-Induced iNOS in Superficial GFAP-Positive Cells Is Attenuated by the Selective iNOS Inhibitor 1400W

Immunohistochemistry confirmed the cellular localization of iNOS in the L4-L5 spinal cord segments of sham-operated, 4-week SCI and 4-week SCI treated with 1400W rats. iNOS-immunoreactivity (IR) colocalized with NeuN-IR across all groups (Figure 6A–C). The percentage of iNOS-IR colocalized with NeuN-IR, relative to the total number of DAPI-stained cells, decreased in both SCI and 1400W-treated SCI rats compared to sham-operated controls ($F = 10.223$, $p < 0.001$, $p = 0.006$, respectively), but showed no significant difference between SCI and 1400W-treated SCI rats (Figure 6D).

iNOS-IR was not observed with GFAP-IR of the sham group (Figure 6E), while it did colocalize with GFAP-IR in the superficial layer of both 4-week post-SCI and 1400W-treated SCI rats (Figure 6F,G). The maximum branch length of GFAP-IR was significantly greater in SCI rats than in sham-operated rats ($F = 21.456$, $p < 0.001$), and significantly lower in 1400W-treated SCI rats than in SCI rats (Figure 6H $p < 0.001$). The integrated density of iNOS in the superficial lamina was significantly increased in SCI rats compared with sham-operated controls ($F = 56.402$, $p < 0.001$), and significantly decreased in 1400W-treated SCI rats compared with SCI rats (Figure 6L $p < 0.001$). However, no colocalization of iNOS with OX42-IR was detected in any group (Figure 6I–K). These results demonstrate that the selective iNOS inhibitor 1400W attenuated iNOS-IR density and reactive astrocyte morphology without affecting neuronal iNOS expression.

4 | Discussion

The present study revealed that iNOS, which is primarily associated with inflammatory processes, plays an important role in below-level neuropathic pain following SCI. Spinal

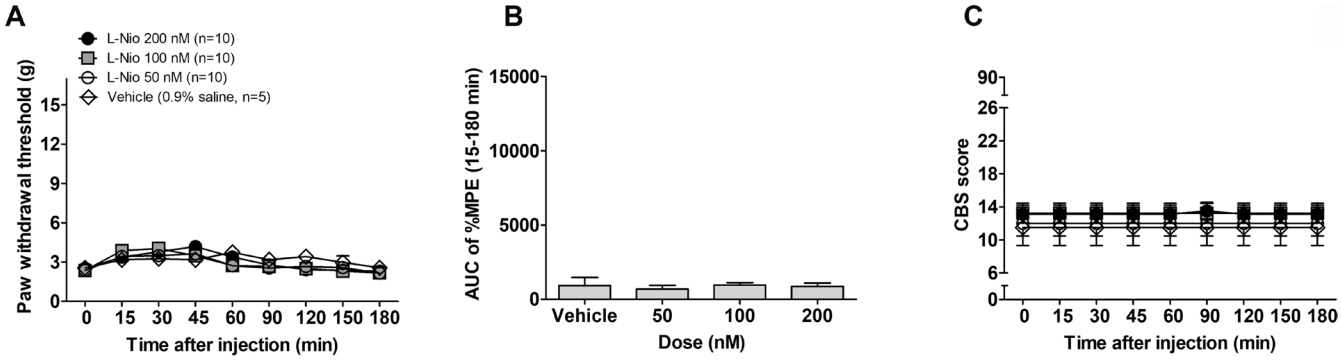

FIGURE 4 | Effect of intrathecal administration of the eNOS inhibitor L-NIO on mechanical paw hypersensitivity in SCI rats. (A) Paw withdrawal thresholds in response to mechanical stimuli following intrathecal administration of vehicle (0.9% saline, open diamonds, $n = 5$) or NPLA at 50 (open circles, $n = 10$), 100 (grey squares, $n = 10$) or 200 nM/5 μL (closed circles, $n = 10$) at 4 weeks post-SCI. (B) AUC calculated from %MPE values. (C) Motor-related side effects assessed by CBS score. All data are presented as mean ± standard error of the mean (SEM).

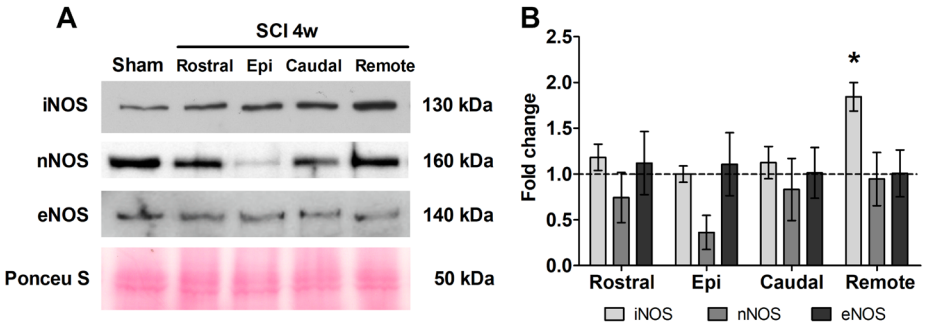

FIGURE 5 | Protein expression of NOS subtypes in the spinal segments following SCI. (A) Representative western blot images showing iNOS, nNOS, eNOS and Ponceau S bands from rostral, epicentre, caudal and remote segments. (B) Bar graph showing quantification of the band intensity (B) for iNOS (light grey), nNOS (middle grey) and eNOS (dark grey) at 4 weeks after SCI ($n = 5$) and sham-operated ($n = 5$). Protein expression was normalised to the sham-operated group (set as 1, dashed line) relative to the Ponceau S band (loading control). All data are presented as mean ± standard error of the mean (SEM). *$p < 0.05$: sham versus SCI.

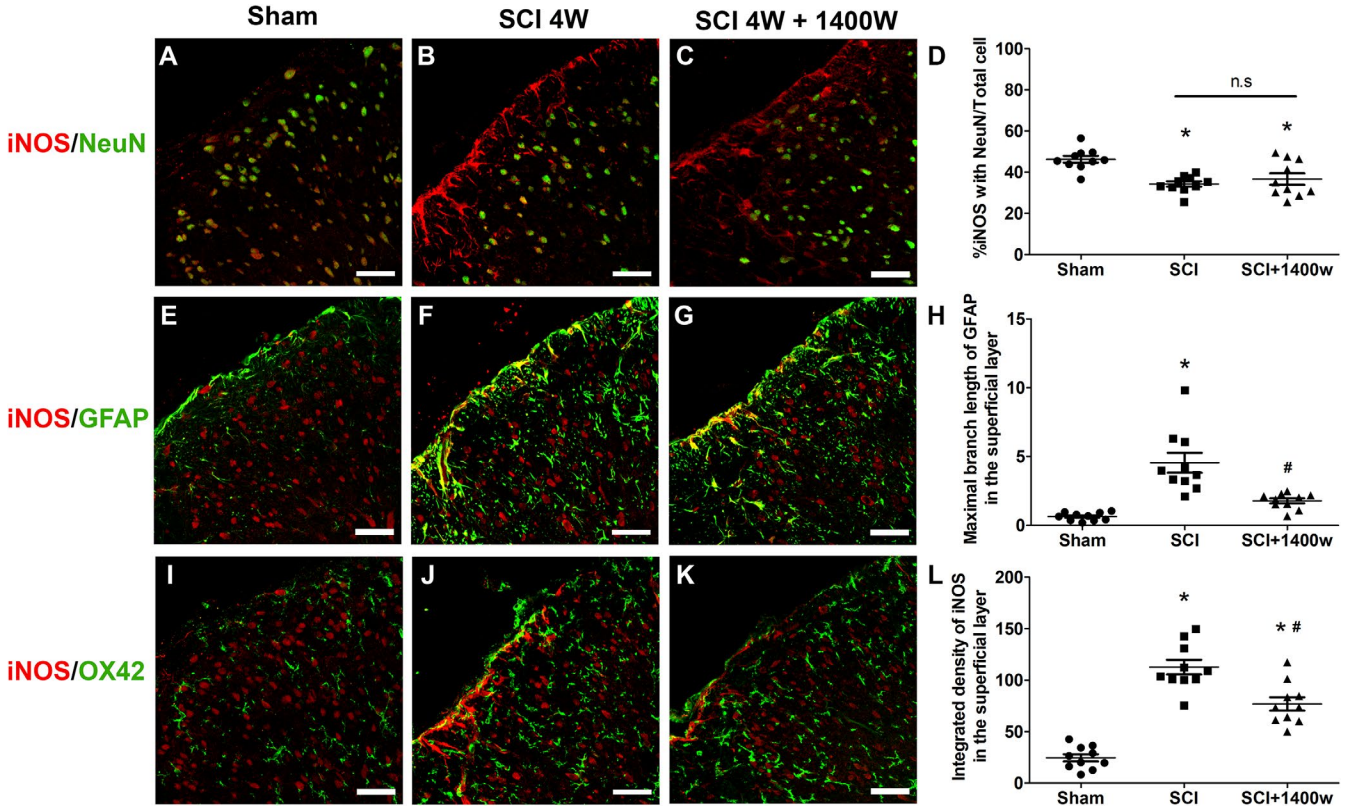

FIGURE 6 | Cellular localisation and quantification of iNOS-IR in the L4-L5 spinal segment following SCI. Representative immunofluorescence images of iNOS-IR (A–C, E–G, I–K; red), NeuN-IR for neurons (A–C; green), GFAP-IR for astrocytes (E–G; green) and OX42-IR for microglia (I–K; green) in the L4-5 spinal segment. Images are representative of sham-operated, 4-week SCI and 4-week SCI with 100 nmol/5 μL 1400W rat group. Scale bar: 50 μm, white. Quantification of confocal images of lamina I-III of the L4-L5 spinal segment (D, H, L) from sham-operated (closed circles), SCI (closed squares) and SCI with 100 nmol/5 μL 1400W groups (closed triangles) was performed using ImageJ. All data are presented as mean ± standard error of the mean (SEM). *$p < 0.05$: sham versus SCI, $^{\#}p < 0.05$: SCI versus SCI with 1400W, n.s: no significance.

contusion induces long-lasting low-grade chronic inflammation that extends beyond the injured epicentre to adjacent rostral and caudal regions (Fleming et al. 2006; Franz et al. 2014). This widespread inflammatory response is accompanied by increased iNOS activity in supraspinal regions (Wang et al. 2022; Xu et al. 2001; Yang et al. 2007). Extending these findings, our study showed that expression of iNOS protein was increased in the remote L4-L5 segment during the chronic phase after spinal contusion injury. Notably, this region innervates the hind paws in rats, which is crucial for below-level pain. This finding suggests that elevated iNOS expression in these regions may be associated with sustained inflammatory processes, potentially contributing to chronic hypersensitivity after SCI.

To determine the cellular localisation of spinal iNOS, we performed immunohistochemical analyses using cellular markers for astrocytes, microglia and neurons.

A critical finding was iNOS-IR in GFAP-positive cells within the superficial layers of the L4-L5 segments after spinal contusion, whereas this pattern was not observed under normal conditions. This result is noteworthy as astrocytes may play a significant role in inflammation due to their direct contact with blood vessels in the central nervous system (CNS) (Lee et al. 2023). Consistent with our findings, Nesic et al. (2005) reported that protein expression of astrocyte activation markers such as GFAP, S100β and AQP4 was more pronounced in the caudal region compared to the rostral region for up to 9 months after spinal contusion in rats. This suggests that astrocyte activation in this region is associated with chronic neuropathic pain. In addition, the mechanism underlying the increased iNOS activity may be linked to increased expression of pro-inflammatory cytokines in astrocytes. Previous studies have demonstrated that pro-inflammatory cytokines activated by canonical NF-κB signalling pathways, such as IL-1β and IFN-γ, stimulate iNOS expression in human primary cultured astrocytes (Arias-Salvatierra et al. 2011; Jana et al. 2005). These results suggest that inhibition of astrocytic iNOS activity could have therapeutic potential for below-level pain in the chronic phase after SCI.

The iNOS-IR was detected in NeuN positive cells in both sham and SCI rats. Similar to our present study, Xu et al. (2001) reported that iNOS-IR was present in neurons and glial cells at the injury site at 7 days after SCI. Duarte- Silva et al. (2021) identified inducible nitric oxide synthase immunoreactivity in neuronal cells within the spinal cord of an experimental autoimmune encephalomyelitis model using the same antibody that was employed in our investigation. In brain tissue, iNOS is detected in both neurons and astrocytes but appears in non-overlapping regions (Cespuglio et al. 2019). Chen et al. (2024) additionally documented congruent results in a rat model of traumatic brain injury utilising an alternative iNOS antibody from Invitrogen (PA1-036). This study noted that neuronal iNOS is expressed at lower levels under non-inflammatory conditions, and its role may differ from that of nNOS. However, it is not possible to definitively exclude the possibility that the iNOS-IR signal observed with NeuN-IR may be non-specific. Nevertheless, the possibility of neuronal iNOS expression cannot be disregarded, given that various studies have documented iNOS-IR in cells that bear resemblance to neurons. Additional studies should be conducted to confirm and expand upon these results.

To investigate the therapeutic potential of NOS inhibition, we examined changes in paw hypersensitivity after administration of a non-selective NOS inhibitor, L-NAME. In our present study, L-NAME effectively reduced paw hypersensitivity, but also induced motor function-related side effects. L-NAME regulates not only the NOS system but also fatty acid oxidation, redox homeostasis and intracellular iron-containing systems (Liu et al. 2019; Peterson et al. 1992). Liu et al. (2019) predominantly examine the function of peroxisomes in adipocytes, particularly their involvement in fatty acid oxidation and the maintenance of redox homeostasis. Although the reference offers significant information on the potential of L-NAME in the regulation of redox processes, it does not explicitly endorse the assertion that L-NAME releases NO. Peterson et al. (1992) investigate the impact of L-NAME on the reduction of cytochrome C within intracellular iron-containing systems. In the current investigation, L-NAME demonstrated efficacy in decreasing paw hypersensitivity, while also producing side effects related to motor function. These references indicate that L-NAME may have unintended effects beyond its primary function as a nitric oxide synthase (NOS) inhibitor.

To overcome the constraints of L-NAME, we investigated specific NOS isoforms involved in regulating abnormal sensitivity after SCI. 1400W demonstrates a high level of selectivity as an inhibitor of inducible nitric oxide synthase (iNOS), showing at least 5000-fold selectivity for iNOS over endothelial NOS (eNOS) and 200-fold selectivity over neuronal NOS (nNOS) (Garvey et al. 1997). Nω-Propyl-L-arginine (NPLA) exhibits significant selectivity towards nNOS, demonstrating an inhibitory potency that is 3000 times higher than that for iNOS and 150 times higher than that for eNOS (Zhang et al. 1997). L-N5-(1-iminoethyl) ornithine (L-NIO) exhibits a favourable selectivity towards inhibiting eNOS in comparison to other NOS isoforms (Jiang et al. 2002; Mulligan et al. 1992; Wolff et al. 1998).

In our present investigation, mechanical hypersensitivity in the paw was diminished within a 3-h timespan upon the inhibition of iNOS in the chronic phase after spinal contusion. This finding suggests that the inhibitory effect on iNOS may only be effective within a 3-h time frame, as no additional improvement was noted after this period. This result represents a significant improvement over systemic administration of 1400W, which requires up to 66 h to reduce paw hypersensitivity due to delayed distribution to the brain (Staunton et al. 2018). Thus, intrathecal 1400W intervention may be helpful to attenuate neuropathic pain as it offers a rapid onset of action with minimal motor-related side effects.

In addition, the increased iNOS hyperactivity within GFAP-positive cells was attenuated by 1400W, which did not affect the neuronal expression of iNOS. This selective effect on astrocytic iNOS, while preserving neuronal iNOS, may be beneficial in maintaining physiological NO signalling in neurons while reducing pathological NO production in reactive astrocytes.

Recently, astrocytes are categorised into five subpopulations (A-E types) that display varying distributions across the CNS region and perform distinct functions (Allahyari et al. 2022; Batiuk et al. 2020). They have diverse functions to support neuronal functions, including metabolic and nutrient support, maintenance of ion homeostasis, neurotransmitter buffering and involvement in the inflammatory process for neuron repair. This highlights the importance of selectively regulating the function of astrocytes. Among these subtypes, Hes5 positive astrocytes belonging to subtype A are distributed in the dorsal horn of the spinal cord. Activation of these astrocytes is associated with the manifestation of allodynia-like behaviour (Sueto et al. 2024). On the other hand, activated astrocytes release not only pro-inflammatory cytokines but also anti-nociceptive substances such as IL-27, Lamp1, or Trail (Lee et al. 2023; Xu et al. 2021). Therefore, the specific regulation of iNOS-expressing astrocytes via intrathecal 1400W administration may be a more effective approach to mitigating paw hypersensitivity in comparison to the use of broad-spectrum astrocyte inhibitors. Suppression of the entire astrocyte population could potentially impact various functions of astrocytes, including pain modulation. As a result, it is generally likely that

the behavioural outcomes will deviate from initial expectations. At present, there is a lack of pharmacological interventions that target astrocytes based on their specific subtypes. Hence, it would be worthwhile to study their potential use in the event that such medications are produced in the future.

In contrast to iNOS, we found no changes in either constitutive NOS (cNOS: nNOS or eNOS) expression in caudal regions after spinal contusive injury. We also injected NPLA or L-Nio to inhibit nNOS and eNOS, respectively. There was no significant reduction in hypersensitivity observed with intrathecal nNOS or eNOS antagonists, as opposed to iNOS inhibition. These results could potentially be explained by differences in the roles of NO produced by iNOS and cNOS (Xu et al. 2001; Zhao et al. 1998). nNOS is located downstream of the signalling pathway regulated by GluN2B. In our previous study, it was observed that spinal contusive injury did not result in an increase in GluN2B expression or produce significant analgesic effects from GluN2B antagonists, in contrast to findings from the spinal hemisection model (Kim et al. 2012). Thus, it can be concluded that spinal cord contusion-induced paw hypersensitivity may be more influenced by iNOS-related signalling pathways in comparison to eNOS or GluN2B-nNOS signalling.

In conclusion, selective inhibition of astrocytic iNOS represents a promising therapeutic approach for regulating chronic neuropathic pain following SCI. Recently, there has been a trend towards categorising astrocytes into various types based on their diverse functions (Lin et al. 2017). Although the specific type of astrocyte responsible for the overexpression of iNOS was not identified, future research efforts should be directed towards investigating the involvement of distinct subpopulations of astrocytes in neuroinflammation following SCI.

Author Contributions

This study was designed by all authors. The experiments and data analyses were performed by Youngkyung Kim and Hyunggoo Kang. Youngkyung Kim had a primary role in preparing the manuscript, which was edited by Young Wook Yoon. All authors have approved the final version of the manuscript and agree to be accountable for all aspects of the work.

Acknowledgements

This work was supported by two separate grants from the Korea University (K2509181), and the Korea Science and Engineering Foundation (KOSEF), funded by the Ministry of Science and ICT (MSIT; grant number NRF-2022R1F1A1073548).

Conflicts of Interest

The authors declare no conflicts of interest.

References

Allahyari, R. V., N. M. Heinsinger, D. Hwang, et al. 2022. "Response of Astrocyte Subpopulations Following Spinal Cord Injury." *Cells* 11: 721.

Andrabi, S. M., N. S. Sharma, A. Karan, et al. 2023. "Nitric Oxide: Physiological Functions, Delivery, and Biomedical Applications." *Advanced Science* 10: 2303259.

Arias-Salvatierra, D., E. K. Silbergeld, L. C. Acosta-Saavedra, and E. S. Calderon-Aranda. 2011. "Role of Nitric Oxide Produced by iNOS Through NF-κB Pathway in Migration of Cerebellar Granule Neurons Induced by Lipopolysaccharide." *Cellular Signalling* 23: 425–435.

Arribas-López, E., N. Zand, O. Ojo, M. J. Snowden, and T. Kochhar. 2021. "The Effect of Amino Acids on Wound Healing: A Systematic Review and Meta-Analysis on Arginine and Glutamine." *Nutrients* 13: 2498.

Batiuk, M. Y., A. Martirosyan, J. Wahis, et al. 2020. "Identification of Region-Specific Astrocyte Subtypes at Single Cell Resolution." *Nature Communications* 11: 1220.

Beck, P. L., R. Xavier, J. Wong, et al. 2004. "Paradoxical Roles of Different Nitric Oxide Synthase Isoforms in Colonic Injury." *American Journal of Physiology. Gastrointestinal and Liver Physiology* 286: G137–G147.

Boettger, M. K., N. Üceyler, M. Zelenka, et al. 2007. "Differences in Inflammatory Pain in nNOS-, iNOS- and eNOS-Deficient Mice." *European Journal of Pain* 11: 810–818.

Casha, S., D. Zygun, M. D. McGowan, I. Bains, V. W. Yong, and J. R. Hurlbert. 2012. "Results of a Phase II Placebo-Controlled Randomized Trial of Minocycline in Acute Spinal Cord Injury." *Brain* 135: 1224–1236.

Cespuglio, R., D. Amrouni, E. F. Raymond, B. Bouteille, and A. Buguet. 2019. "Cerebral Inducible Nitric Oxide Synthase Protein Expression in Microglia, Astrocytes and Neurons in Trypanosoma Brucei Brucei-Infected Rats." *PLoS One* 14: e0215070.

Chambel, S. S., I. Tavares, and C. D. Cruz. 2020. "Chronic Pain After Spinal Cord Injury: Is There a Role for Neuron-Immune Dysregulation?" *Frontiers in Physiology* 11: 748.

Chaplan, S. R., F. W. Bach, J. W. Pogrel, J. M. Chung, and T. L. Yaksh. 1994. "Quantitative Assessment of Tactile Allodynia in the Rat Paw." *Journal of Neuroscience Methods* 53: 55–63.

Chen, C., Z. H. Chang, B. Yao, et al. 2024. "3D Printing of Interferon γ-Preconditioned NSC-Derived Exosomes/Collagen/Chitosan Biological Scaffolds for Neurological Recovery After TBI." *Bioactive Materials* 39: 375–391.

De Alba, J., N. M. Clayton, S. D. Collins, P. Colthup, L. Chessell, and R. G. Knowles. 2006. "GW274150, a Novel and Highly Selective Inhibitor of the Inducible Isoform of Nitric Oxide Synthase (NOS), Shows Analgesic Effects in Rat Models of Inflammatory and Neuropathic Pain." *Pain* 120: 170–181.

Doyle, T., Z. Chen, C. Muscoli, et al. 2012. "Targeting the Overproduction of Peroxynitrite for the Prevention and Reversal of Paclitaxel-Induced Neuropathic Pain." *Journal of Neuroscience* 32: 6149–6160.

Duarte- Silva, E., S. Meiry da Rocha Araújo, W. H. Oliveira, et al. 2021. "Sildenafil Alleviates Murine Experimental Autoimmune Encephalomyelitis by Triggering Autophagy in the Spinal Cord." *Frontiers in Immunology* 12: 671511.

Finnerup, N. B., C. Norrbrink, K. Trok, et al. 2014. "Phenotypes and Predictors of Pain Following Traumatic Spinal Cord Injury: A Prospective Study." *Journal of Pain* 15: 40–48.

Fleming, J. C., M. D. Norenberg, D. A. Ramsay, et al. 2006. "The Cellular Inflammatory Response in Human Spinal Cords After Injury." *Brain* 129: 3249–3269.

Förstermann, U., and W. C. Sessa. 2012. "Nitric Oxide Synthases: Regulation and Function." *European Heart Journal* 33: 829–837.

Franz, S., M. Ciatipis, K. Pfeifer, et al. 2014. "Thoracic Rat Spinal Cord Contusion Injury Induces Remote Spinal Gliogenesis but Not Neurogenesis or Gliogenesis in the Brain." *PLoS One* 9: e102896.

Freire, M. A. M., J. S. Guimarães, W. Gomes-Leal, and A. Pereira. 2009. "Pain Modulation by Nitric Oxide in the Spinal Cord." *Frontiers in Neuroscience* 3: 175–181.

Gale, K., H. Kerasidis, and J. R. Wrathall. 1985. "Spinal Cord Contusion in the Rat: Behavioral Analysis of Functional Neurologic Impairment." *Experimental Neurology* 88: 123–134.

Garvey, E. P., J. A. Oplinger, E. S. Furfine, et al. 1997. "1400W Is a Slow, Tight Binding, and Highly Selective Inhibitor of Inducible Nitric-Oxide Synthase In Vitro and In Vivo." *Journal of Biological Chemistry* 272: 4959–4963.

Jana, M., J. A. Anderson, R. N. Saha, X. Liu, and K. Pahan. 2005. "Regulation of Inducible Nitric Oxide Synthase in Proinflammatory Cytokine-Stimulated Human Primary Astrocytes." *Free Radical Biology and Medicine* 38: 655–664.

Jiang, M. H., T. Kaku, J. Hada, and Y. Hayashi. 2002. "Different Effects of eNOS and nNOS Inhibition on Transient Forebrain Ischemia." *Brain Research* 946: 139–147.

Kim, H. Y., H. J. Lee, T. L. Kim, et al. 2020. "Prevalence and Characteristics of Neuropathic Pain in Patients With Spinal Cord Injury Referred to a Rehabilitation Center." *Annals of Rehabilitation Medicine* 44: 438–449.

Kim, Y., H. Y. Cho, Y. J. Ahn, J. Kim, and Y. W. Yoon. 2012. "Effect of NMDA NR2B Antagonist on Neuropathic Pain in Two Spinal Cord Injury Models." *Pain* 153: 1022–1029.

Kim, Y., K.-W. Park, E. Lee, and Y. W. Yoon. 2023. "Inhibition of Neuronal Peroxisome Proliferator-Activated Receptor-γ Attenuates Motor Function Improvement After Spinal Cord Injury in Rats." *European Journal of Neuroscience* 57: 1466–1480.

Kim, Y., K.-W. Park, J. Oh, J. Kim, and Y. W. Yoon. 2019. "Alterations in Protein Expression Patterns of Spinal Peroxisome Proliferator-Activated Receptors After Spinal Cord Injury." *Neurological Research* 41: 883–892.

Komirishetty, P., A. Areti, V. K. Arruri, R. Sistla, R. Gogoi, and A. Kumar. 2021. "FeTMPyP a Peroxynitrite Decomposition Catalyst Ameliorated Functional and Behavioral Deficits in Chronic Constriction Injury Induced Neuropathic Pain in Rats." *Free Radical Research* 55: 1005–1017.

Lackovic, J., V. Jeevakumar, M. Burton, T. J. Price, and G. Dussor. 2023. "Peroxynitrite Contributes to Behavioral Responses, Increased Trigeminal Excitability, and Changes in Mitochondrial Function in a Preclinical Model of Migraine." *Journal of Neuroscience* 43: 1627–1642.

Lee, H.-G., J.-H. Lee, L. E. Flausino, and F. J. Quintana. 2023. "Neuroinflammation: An Astrocyte Perspective." *Science Translational Medicine* 15: eadi7828.

Lee, W. H., L. L. Li, A. Chawla, et al. 2018. "Disruption of nNOS-NOS1AP Protein-Protein Interactions Suppresses Neuropathic Pain in Mice." *Pain* 159: 849–863.

Li, Z. F., H. Y. Bai, R. Y. Zhang, et al. 2022. "Systematic Analysis of Critical Genes and Pathways Identified a Signature of Neuropathic Pain After Spinal Cord Injury." *European Journal of Neuroscience* 56: 3991–4008.

Liang, Y., Y. Ma, J. Wang, et al. 2021. "Leptin Contributes to Neuropathic Pain via Extrasynaptic NMDAR-nNOS Activation." *Molecular Neurobiology* 58: 1185–1195.

Lin, J., C. C. Lin, K. Yu, et al. 2017. "Identification of Diverse Astrocyte Populations and Their Malignant Analogs." *Nature Neuroscience* 20: 396–405.

Liu, J., W. Lu, B. Shi, S. Klein, and X. Su. 2019. "Peroxisomal Regulation of Redox Homeostasis and Adipocyte Metabolism." *Redox Biology* 24: 101167.

Marques, S. I., H. Carmo, F. Carvalho, S. I. Sá, and J. P. Silva. 2023. "A Semi-Automatic Method for the Quantification of Astrocyte Number and Branching in Bulk Immunohistochemistry Images." *International Journal of Molecular Sciences* 24: 4508.

Mulligan, M. S., S. Moncada, and P. A. Ward. 1992. "Protective Effects of Inhibitors of Nitric Oxide Synthase in Immune Complex-Induced Vasculitis." *British Journal of Pharmacology* 107: 1159–1162.

Murphy, S., M. L. Simmons, L. Agullo, et al. 1993. "Synthesis of Nitric Oxide in CNS Glial Cells." *Trends in Neurosciences* 16: 323–328.

Nesic, O., J. Lee, K. M. Johnson, et al. 2005. "Transcriptional Profiling of Spinal Cord Injury-Induced Central Neuropathic Pain." *Journal of Neurochemistry* 95: 998–1014.

Osuka, K., Y. Watanabe, T. Takagi, et al. 2008. "Activation of Endothelial Nitric Oxide Synthase Following Spinal Cord Injury in Mice." *Neuroscience Letters* 436: 265–268.

Paterniti, I., E. Esposito, E. Mazzon, P. Bramanti, and S. Cuzzocrea. 2011. "Evidence for the Role of PI(3)-Kinase-AKT-eNOS Signalling Pathway in Secondary Inflammatory Process After Spinal Cord Compression Injury in Mice." *European Journal of Neuroscience* 33: 1411–1420.

Pertovaara, A., and H. Breivik. 2016. "Pain Treatment With Intrathecal Corticosteroids: Much Ado About Nothing? But Epidural Corticosteroids for Radicular Pain Is Still an Option." *Scandinavian Journal of Pain* 10: 82–84.

Peterson, D. A., D. C. Peterson, S. Archer, and E. K. Weir. 1992. "The Non Specificity of Specific Nitric Oxide Synthase Inhibitors." *Biochemical and Biophysical Research Communications* 187: 797–801.

Pfyffer, D., P. O. Wyss, E. Huber, A. Curt, A. Henning, and P. Freund. 2020. "Metabolites of Neuroinflammation Relate to Neuropathic Pain After Spinal Cord Injury." *Neurology* 95: e805–e814.

Safdarian, M., E. Trinka, V. Rahimi-Movaghar, et al. 2023. "Global, Regional, and National Burden of Spinal Cord Injury, 1990–2019: A Systematic Analysis for the Global Burden of Disease Study 2019." *Lancet Neurology* 22: 1026–1047.

Staunton, C. A., R. Barrett-Jolley, L. Djouhri, and T. Thippeswamy. 2018. "Inducible Nitric Oxide Synthase Inhibition by 1400W Limits Pain Hypersensitivity in a Neuropathic Pain Rat Model." *Experimental Physiology* 103: 535–544.

Sueto, D., A. Onishi, Y. Yoshikawa, and M. Tsuda. 2024. "Laminar-Selective Spinal Astrocyte Population Capable of Converting Tactile Information Into Nociceptive in Rats." *Journal of Pharmacological Sciences* 154: 312–315.

Thomas, D. D., X. Liu, S. P. Kantrow, and J. R. Lancaster Jr. 2001. "The Biological Lifetime of Nitric Oxide: Implications for the Perivascular Dynamics of NO and O2." *Proceedings of the National Academy of Sciences of the United States of America* 98: 355–360.

Van Slooten, A. R., Y. Sun, A. N. Clarkson, and B. J. Connor. 2015. "L-NIO as a Novel Mechanism for Inducing Focal Cerebral Ischemia in the Adult Rat Brain." *Journal of Neuroscience Methods* 245: 44–57.

Varghese, S. N., O. C. Eller, E. E. Young, and K. M. Baumbauer. 2024. "Spinal Cord Injury-Induced Chronic Pain Is Driven by a Central to Peripheral Interleukin-1 Mediated Signaling Pathway." *Journal of Pain* 25: 21.

Wang, L., M. A. Gunduz, A. T. Semeano, et al. 2022. "Coexistence of Chronic Hyperalgesia and Multilevel Neuroinflammatory Responses After Experimental SCI: A Systematic Approach to Profiling Neuropathic Pain." *Journal of Neuroinflammation* 19: 264.

Wolff, D. J., A. Lubeskie, D. S. Gauld, and M. J. Neulander. 1998. "Inactivation of Nitric Oxide Synthases and Cellular Nitric Oxide Formation by N6-Iminoethyl-L-Lysine and N5-Iminoethyl-L-Ornithine." *European Journal of Pharmacology* 350: 325–334.

Xu, J., G. M. Kim, S. Chen, et al. 2001. "iNOS and Nitrotyrosine Expression After Spinal Cord Injury." *Journal of Neurotrauma* 18: 523–532.

Xu, Q., N. C. Ford, S. He, et al. 2021. "Astrocytes Contribute to Pain Gating in the Spinal Cord." *Science Advances* 7: eabi6287.

Yang, J. Y., H. S. Kim, and J. K. Lee. 2007. "Changes in Nitric Oxide Synthase Expression in Young and Adult Rats After Spinal Cord Injury." *Spinal Cord* 45: 731–738.

Yoon, Y. W., B. Sung, and J. W. Chung. 1998. “Nitric Oxide Mediates Behavioral Signs of Neuropathic Pain in an Experimental Rat Model.” *Neuroreport* 9: 367–372.

Zhang, H. Q., W. Fast, M. A. Marletta, P. Martasek, and R. B. Silverman. 1997. “Potent and Selective Inhibition of Neuronal Nitric Oxide Synthase by Nω-Propyl-l-Arginine.” *Journal of Medicinal Chemistry* 40: 3869–3870.

Zhao, M.-L., J. S. H. Liu, D. He, D. W. Dickson, and S. C. Lee. 1998. “Inducible Nitric Oxide Synthase Expression Is Selectively Induced in Astrocytes Isolated From Adult Human Brain.” *Brain Research* 813: 402–405.

Zhou, L., and D. Y. Zhu. 2009. “Neuronal Nitric Oxide Synthase: Structure, Subcellular Localization, Regulation, and Clinical Implications.” *Nitric Oxide* 20: 223–230.